Journal of the Civil Engineering Forum, May 2022, 8(2):205-216
DOI 10.22146/jcef.3872
Available Online at https://jurnal.ugm.ac.id/jcef/issue/archive

Numerical Simulation for One-Dimensional (1D) Wave Propagation by Solving the Shallow Water Equations using the Preissmann Implicit Scheme

Prilla Lidyana, Bobby Minola Ginting*, Doddi Yudianto
Department of Civil Engineering, Parahyangan Catholic University, Jl. Ciumbuleuit No.94, Bandung 40141
*Corresponding author: bobbyminola.g@unpar.ac.id

SUBMITTED 26 January 2022 **REVISED** 16 March 2022 **ACCEPTED** 18 March 2022

ABSTRACT This research simulated one-dimensional wave propagation by solving the shallow water equations using the Preissman implicit numerical scheme due to its ability to maintain simplicity and stability at a larger time step value. This numerical model was fundamentally developed to satisfy the shallow water condition, where the water depth or horizontal-length scale is much smaller than the free-surface disturbance wavelength or vertical-length scale, and to comprehensively test the accuracy of the model. Consequently, three different types of waves were considered and these include (1) tidal, (2) roll, and (3) solitary. In the first case, the model was proven to be robust and accurate due to its relatively-small errors for both water-surface elevation and velocity indicating that the Preismann scheme is suitable for longwave simulations. In the second case, it was fairly accurate in capturing the periodic permanent roll waves despite showing a higher water-surface elevation than the one observed and this discrepancy is due to the neglect of the turbulent Reynold stress in the model. Meanwhile, the last case showed remarkable discrepancies in the water-surface elevation because the dispersion effect is quite significant during the wave propagation. This indicates that the Preismann scheme underestimated the wave crest along with time when the dispersion term was neglected. All simulations were performed using the tridiagonal matrix algorithm, thereby eliminating the need for iterations for the solution of the Preismann scheme. The findings of this study are beneficial to the next generation of the Preissmann-scheme models which can be designed to include turbulence and dispersion terms.

KEYWORDS Preissmann scheme; Roll wave; Shallow water equations; Solitary wave; Tidal wave; Wave propagation.

1 INTRODUCTION

Almost all phenomena in the coastal zone are actively dominated by waves, thereby, becoming the most concerning aspect of infrastructure design. It was found that these waves are caused by several external and internal factors such as wind, the geometry of the sea, astronomical tide, earthquake on the seabed, and others (Pratomo et al., 2016). Wind is the most apparent factor in generating waves followed by the astronomical tide caused by the gravitational attraction between the earth, sun, and moon. Meanwhile, the less important waves capable of causing great losses in some places are those generated seismically through tsunamis and by moving vessels (Sorensen, 2006).

Significant improvements have recently been made in describing and predicting wave propagation processes in shallow water numerical modeling, and this concept is based on the smallness of the ratio between water depth and wavelength. This modeling process is classified into two groups which are dispersion and non-dispersion which typically deal with the shallow water equations (SWE) in either primitive or conservative form. It is important to note that the dispersion and non-dispersion models lie on the non-hydrostatic term included in the SWE in the form of Boussinesq-type models, non-hydrostatic shallow water, or vertically averaged and moment equations as explained in (Ginting and Ginting, 2020).

The SWE dispersion model is suitable to simulate the deep-water or short wave, specifically where its speed depends on the wavelength. This causes the vertical-length scale to be much greater than the horizontal one, to an extent that the non-hydrostatic effects cannot be neglected. However, the non-dispersion is suitable for simulating shallow-water or long waves, where its speed is independent of the wavelength. It was discovered that the vertical velocity component does not affect the pressure distribution thereby satisfying the hydrostatic assumption. Based on this explanation, the SWE dispersion model is suitable for modeling both short and longwave modeling specifically for those that involve transformation processes from the deep to the shallow water.

A non-dispersion model is still a common approach for practical purposes and in coastal applications because it has a computational cost that is 3 to 4 times lower than that of dispersion. An example is seen in the recent work of Audusse et al. (2019), where both models were compared in simulating tsunami waves generated by a landslide, and was discovered that the non-dispersion model performs better than that of dispersion in the generation zone but conversely in the propagation zone. Moreover, the non-dispersion model produces much less computational cost in terms of complexity compared to that of dispersion. Further examples of accurate prediction for tsunami propagation using the non-dispersion model are shown in (Ginting and Mundani, 2019; Arcos and LeVeque, 2015; Meister et al., 2016). Therefore, the decision to either use the dispersion or non-dispersion model depends on the modeling requirements.

In this present research, the one-dimensional SWE derived from the Navier-Stokes equations was utilized to describe the fluid motion based on the conservation of mass and momentum. This has a dispersive effect which is neglected in the SWE when the uniform distribution value of vertical velocity and hydrostatic pressure is assumed. Based on this, Preissmann's implicit scheme which is found to be stable over larger values is employed to numerically solve the 1D SWE, and to model the wave propagation that typically includes a long simulation time. It is important to note that this Preissmann scheme has been applied to several popular commercial and non-commercial codes, such as DUFLOW (Clemmens et al., 1993) and HEC-RAS (Brunner and USACE, 2016). These two findings discovered that the solutions of the Preissmann scheme may have false oscillations, particularly when the flow conditions shifted from free-surface to pressurized flow.

A study by An et al. (2018) proposed a new hybrid numerical solution to solve this problem by combining the upwind and centered flux solver. Although the Preissmann scheme is generally created for non-transcritical flows, Sart et al. (2010) employed it to solve transcritical flows by modifying the formulation only in transcritical zones while maintaining its conservative properties. This present study aims to investigate the accuracy of the in-house codes by utilizing the Preissmann scheme against the three cases of the wave propagation problem. The first case is to simulate the tidal wave, which is typically a long wave problem, and the second is focused on simulating the roll wave propagation being periodically permanent over the time, while the third entails the simulation of the solitary wave with the aim of observing the largest discrepancy produced by the scheme for incorporating the dispersion effect. In these simulations, the tridiagonal matrix algorithm is applied to the solution of the Preissmann scheme, thereby eliminating the need for iterations.

2 METHOD

This research begins with several related literature reviews followed by the solution of the one-dimensional SWE by developing an in-house code with Preissmann's implicit scheme which was written in Fortran and compiled using the Intel Fortran compiler 64-Bit version 2020. The code is subsequently tested and compared with some benchmark cases related to the simulations of wave propagation. Figure 1 represents the flow chart of the research methodology.

The results of the comparison test with other benchmarks are further compared with the measured data obtained from the other published journals to show the relationship between the numerical models developed using the Preissmann scheme and other methods.

2.1 Governing Equations

The SWE has been widely used as the governing equation for modeling open channel flows. Meanwhile, by neglecting the vertical acceleration and the translational motion of fluid elements, the

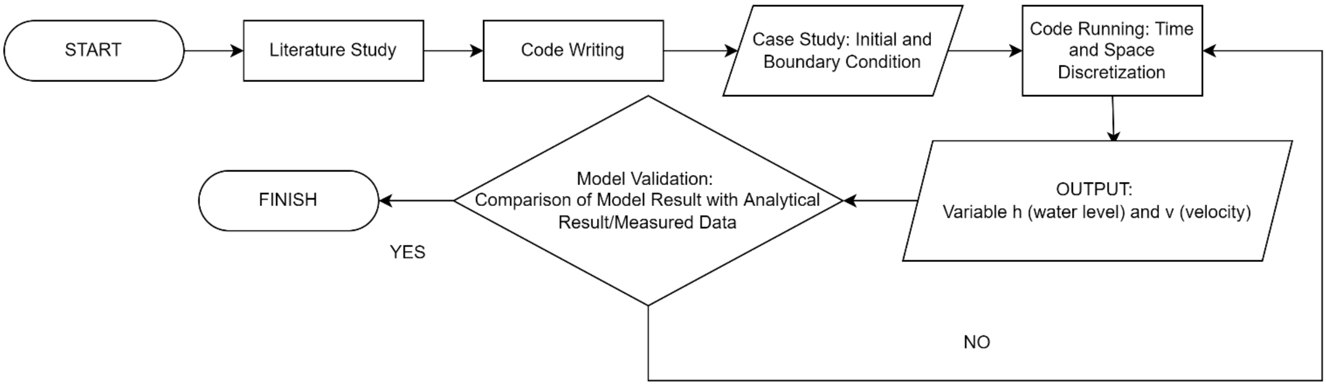

Figure 1 Research Flowchart

mass conservation or continuity and the momentum equations in the 1D form are described as follows:

$$\frac{\partial A}{\partial t} + \frac{\partial Q}{\partial x} = 0 \quad (1)$$

$$\frac{1}{A}\frac{\partial Q}{\partial t} + \frac{1}{A}\frac{\partial}{\partial x}\left(\beta\frac{Q^2}{A}\right) + g\frac{\partial \eta}{\partial x} - gS_0 + g\frac{Q|Q|}{K} = 0 \quad (2)$$

where the discharge, wetted area, and water depth are denoted by Q, A, and η respectively. The variable β is the Boussinesq coefficient and it is equated to 1, g is the gravity acceleration t is the time, S_0 is the bed slope, and $K = n_m^2 \mathrm{A}^2 \mathrm{R}^{4/3}$, where n_m is the Manning coefficient and R is the hydraulic radius of the channel.

2.2 Preissmann Scheme

The SWE, written as a partial differential equation, is discretized by using the Preissmann scheme and this implicit finite-difference method is unconditionally stable and suitable for modeling phenomena that have a long simulation time (Chollet and Cunge, 1980) as seen in Figure 2.

The following is the basic formulation of the Preissmann scheme:

$$f\left(x,t\right) \approx \frac{\theta}{2}\left(f_{j+1}^{n+1} + f_j^{n+1}\right) + \frac{1-\theta}{2}\left(f_{j+1}^{n} + f_j^{n}\right) \quad (3)$$

$$\frac{\partial f}{\partial x} \approx \theta\left(\frac{f_{j+1}^{n+1} f_j^{n+1}}{\Delta x}\right) + \left(1-\theta\right)\left(\frac{f_{j+1}^{n} f_j^{n}}{\Delta x}\right) \quad (4)$$

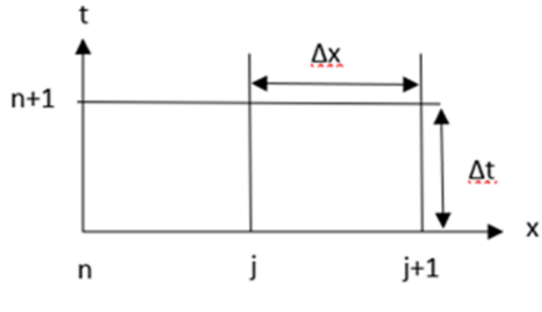

Figure 2 The Preissmann Implicit Scheme

$$\frac{\partial f}{\partial t} \approx \frac{f_{j+1}^{n+1} - f_{j+1}^{n} + f_j^{n+1} - f_j^{n}}{2\Delta t} \quad (5)$$

Where, $f(x,t)$ is an unknown variable including Q, A, and h, together with its temporal and spatial derivatives. The variable θ is a weighting factor with a value between 0.5 and 1, the superscript n refers to the time axis, while the subscript j refers to the spatial axis x.

2.3 Discretization of Governing Equations

The first step of using the Preissmann scheme is to discretize the continuity equations as follows:

$$\frac{\partial A}{\partial t} + \frac{\partial Q}{\partial x} = q, B\frac{\partial \eta}{\partial t} + \frac{\partial Q}{\partial x} = q \quad (6)$$

$$\left\{\frac{\theta}{2}\left(B_{j+1}^{n+1}+B_{j}^{n+1}+\frac{(1-\theta)}{2}\left(B_{J+1}^{n}+B_{j}^{n}\right)\right)\right\}$$
$$\left\{\frac{\eta_{J+1}^{n+1}-\eta_{j+1}^{n}+\eta_{j}^{n+1}-\eta_{j}^{n}}{2\Delta t}\right\}+$$
$$\left\{\theta\left(\frac{Q_{j+1}^{n+1}-Q_{j}^{n+1}}{\Delta x}\right)+\left(1-\theta\right)\left(\frac{Q_{j+1}^{n}-Q_{j}^{n}}{\Delta x}\right)\right\}$$
$$=\left\{\frac{\theta}{2}\left(q_{j+1}^{n+1}+q_{j}^{n+1}\right)+\left(\frac{1-\theta}{2}\right)\left(1_{j+1}^{n}+q_{j}^{n}\right)\right\} \quad (7)$$

Since B and q are the channel width and discharge per unit width, respectively, the above equations are converted into:

$$a_j\Delta\eta_{j+1}+b_j\Delta Q_{j+1}=c_j\Delta\eta_j+d_j\Delta Q_j+G_j \quad (8)$$

$a_j=\frac{\overline{B}}{2\Delta t}, b_j=\frac{\theta}{\Delta x}, C_j=\frac{\overline{-B}}{2\Delta x}, d_j=\frac{\theta}{\Delta x}, G_j=q-\frac{Q_{j+1}^{n}}{\Delta x}+\frac{Q_j^n}{\Delta x}$

The next step is to discretize the momentum equations, written as follows:

$$\frac{\partial Q}{\partial t}+\frac{\partial}{\partial x}\left(\frac{Q^2}{A}\right)+gA\frac{\partial\eta}{\partial x}-gAS_0+gA\frac{Q|Q|}{K}=0 \quad (9)$$

Afterwards, the first term of Equation 9 is discretized as:

$$\frac{\partial Q}{\partial t}=\frac{Q_{j+1}^{n+1}-Q_{j+1}^{n}+Q_{j}^{n+1}-Q_{j}^{n}}{2\Delta t} \quad (10)$$

Meanwhile, the Vonvey's variant of Preissmann is written as A = $\frac{A_{j+1}^{n+1/2}+A_{j}^{n+1/2}}{2}$ is used, hence:

$$\frac{\partial}{\partial x}\left(\beta\frac{Q^2}{A}\right)=\frac{\beta}{\Delta x}\left(\frac{Q_{j+1}^{n+1}Q_{j+1}^{n}}{A_{j+1}^{n+1/2}}-\frac{Q_{j}^{n}Q_{j}^{n+1}}{A_{j}^{n+1/2}}\right) \quad (11)$$

$$gA\frac{\partial\eta}{\partial x}=g\left(\frac{A_{j+1}^{n+1/2}+A_{j}^{n+1/2}}{2}\right)$$
$$\left\{\theta\frac{\eta_{j+1}^{n+1}-\eta_{j}^{n+1}}{\Delta x}+(1-\theta)\left(\frac{\eta_{j+1}^{n}-\eta_{j}^{n}}{\Delta x}\right)\right\} \quad (12)$$

$$gAS_0=g\left(\frac{A_{j+1}^{n+1/2}+A_{j}^{n+1/2}}{2}\right)S_0 \quad (13)$$

$$gA\frac{Q|Q|}{K}=g\left(\frac{A_{j+1}^{n+1/2}+A_{j}^{n+1/2}}{2}\right)\left(\frac{|Q_j^n|Q_j^{n+1}}{K_j^{n+1}}+\frac{|Q_{j+1}^n|Q_{j+1}^{n+1}}{K_{j+1}^{n+1/2}}\right) \quad (14)$$

Furthermore, the four equations above are converted into the form:

$$a_j^*\Delta\eta_{j+1}+b_j^*\Delta Q_{j+1}+c_j^*\Delta Q_{j+1}+d_j^*\Delta Q_j+G_j^* \quad (15)$$

The Taylor series below is firstly used before converting into the form of Equation 15:

$$f\left(t+\Delta t\right)\approx f(t)+\frac{\partial f}{\partial t}\Delta t+\ldots \quad (16)$$

Thus, $f_{j+1}^{n+1}=f_{j+1}^{n}+\Delta f_{j+1}$, and $f_j^{n+1}=f_j^n+\Delta f_j$.

When the Taylor series is applied to Equation 10 – Equation 14, it yields:

$$\frac{\partial Q}{\partial t}=\frac{\Delta Q_{j+i}}{2\Delta t}+\frac{\Delta Q_j}{2\Delta t} \quad (17)$$

$$\frac{\partial}{\partial x}\left(\beta\frac{Q^2}{A}\right)=\frac{\beta}{\Delta x}\left(\frac{(Q_{j+1}^n+\Delta Q_{j+1})Q_{j+1}^n}{A_{j+1}^{n+1/2}}-\frac{(Q_j^n+\Delta Q_j)Q_j^n}{A_j^{n+1/2}}\right)$$
$$=\frac{\beta}{\Delta x}\left(\frac{(Q_{j+1}^n)^2+(Q_{j+1}^n\Delta Q_{j+1})}{A_{j+1}^{n+1/2}}-\frac{(Q_j^n)^2+(Q_j^n\Delta Q_j)}{A_j^{n+1/2}}\right) \quad (18)$$

$$gA\frac{\partial\eta}{\partial x}=g\left(\frac{A_{j+1}^{n+1/2}+A_{j}^{n+1/2}}{2}\right)$$
$$\left\{\frac{\theta}{\Delta x}\left(\Delta\eta_{j+1}\right)-\frac{\theta}{\Delta x}(\eta_j)+\frac{1}{\Delta x}\left(\eta_{j+1}^n-\eta_j^n\right)\right\} \quad (19)$$

$$gA\frac{Q|Q|}{K}=g\left(\frac{A_{j+1}^{n+1/2}+A_{j}^{n+1/2}}{2}\right)$$
$$\left(\frac{|Q_j^n|(Q_j^n+\Delta Q_j)}{K_j^{n+1/2}}+\frac{|Q_{j+1}^n|(Q_{j+1}^n+\Delta Q_{j+1})}{K_{j+1}^{n+1/2}}\right)=$$
$$g\left(\frac{A_{j+1}^{n+1/2}+A_{j}^{n+1/2}}{2}\right)\left\{\frac{(|Q_j^n|Q_j^n+|Q_j^n|\Delta Q_j)}{K_j^{n+1/2}}\right\}+ \quad (20)$$
$$\frac{|Q_{j+1}^n|Q_{j+1}^n+|Q_{j+1}^n|\Delta Qj+1}{K_{j+1}^{n+1/2}}$$

Subsequently, Equation 15 can be written as: $a_j^* = gA\frac{\theta}{\Delta x}, b_j^* = \frac{1}{2\Delta t} + \frac{\beta}{\Delta x}\frac{Q_{j+1}^n}{A_{j+1}^{n+1/2}} + \frac{g}{2}\frac{|Q_{j+1}^n|}{K_{j+1}^{n+1/2}}, c_j^* = gA\frac{\theta}{\Delta x},$
$d_j^* = \frac{-1}{2\Delta t} + \frac{\beta}{\Delta x}\frac{Q_j^n}{A_j^{n+1/2}} - \frac{g}{2}\frac{|Q_j^n|}{K_j^{n+1/2}}$

$G_j^* = \frac{-\beta}{\Delta x}\frac{(Q_{j+1}^n)^2}{A_{j+1}^{n+1/2}} + \frac{\beta}{\Delta x}\frac{(Q_j^n)^2}{A_j^{n+1/2}} - gA\left\{\frac{1}{\Delta x}(\eta_{j+1}^n - \eta_j^n)\right\} - \frac{g}{2}\left\{\frac{|Q_j^n|Q_j^n}{K_j^{n+1/2}} + \frac{|Q_{j+1}^n|Q_{j+1}^n}{K_{j+1}^{n+1/2}}\right\}$

Afterwards, the two general equations, 8 and 15 will be reviewed, starting with Equation 8:

$$a_j\left(\eta_{j+1}^{n+1} - \eta_{j+1}^n\right) + b_j\left(Q_{j+1}^{n+1} - Q_{j+1}^n\right) = c_j\left(\eta_j^{n+1} - \eta_j^n\right) + d_j\left(Q_j^{n+1} - Q_j^n\right) + G_j \quad (21)$$

$$a_j\eta_{j+1}^{n+1} + b_jQ_{j+1}^{n+1} - c_j\eta_j^{n+1} - d_jQ_j^{n+1} = a_j\eta_{j+1}^n + b_jQ_{j+1}^n - c_j\eta_j^n - d_jQ_j^n + G_j \quad (22)$$

Also, Equation 16 is rewritten as:

$$a_j^*\left(\eta_{j+1}^{n+1} - \eta_{j+1}^n\right) + b_j^*\left(Q_{j+1}^{n+1} - Q_{j+1}^n\right) = c_j^*\left(\eta_j^{n+1} - \eta_j^n\right) + d_j^*\left(Q_j^{n+1} - Q_j^n\right) + G_j^* \quad (23)$$

$$a_j^*\eta_{j+1}^{n+1} + b_j^*Q_{j+1}^{n+1} - c_j^*\eta_j^{n+1} - d_j^*Q_j^{n+1} = a_j^*\eta_j^{n+1} + b_j^*Q_{j+1}^n - c_j^*\eta_j^n - d_j^*Q_j^n + G_j^* \quad (24)$$

By summing Equation 22 with Equation 24, the following is obtained:

$$(a_j + a_j^*)\eta_{j+1}^{n+1} + (b_j + b_j^*)Q_{j+1}^{n+1} - (c_j + c_j^*)\eta_j^{n+1} - (d_j + d_j^*)Q_j^{n+1} = (a_j + a_j^*)\eta_{j+1}^n + (b_j + b_j^*)Q_{j+1}^n - (c_j + c_j^*)\eta_j^n - (d_j + d_j^*)Q_j^n + (G_j + G_j^*) \quad (25)$$

By considering $(a_j + a_j^*) = (\overline{a}_j)$, where j = 1 and j = 2 are taken as example:

$$\overline{a_1}\eta_2^{n+1} + \overline{b_1}Q_2^{n+1} + \overline{c_1}\eta_1^{n+1} + \overline{d_1}Q_1^{n+1} = \overline{a_1}\eta_2^n + \overline{b_1}Q_2^n + \overline{c_1}\eta_1^n + \overline{d_1}Q_1^n + (G_1) \quad (26)$$

$$\overline{a_2}\eta_3^{n+1} + \overline{b_2}Q_3^{n+1} + \overline{c_2}\eta_2^{n+1} + \overline{d_2}Q_2^{n+1} = \overline{a_2}\eta_3^n + \overline{b_2}Q_3^n + \overline{c_2}\eta_2^n + \overline{d_2}Q_2^n + (G_2) \quad (27)$$

The formulations above do not produce a tridiagonal matrix, and therefore, another solution must be found by assuming a linear relationship, which is by substituting the equations $\Delta Q_j = E_j\Delta\eta_j + F_j$ into Equation 8 and Equation 15, to yield:

$$a_j\Delta\eta_{j+1} + b_jQ_{j+1} = \left(c_j + d_jE_j\right)\Delta\eta_j^n + d_jF_j + G_j \quad (28)$$

$$a_j^*\Delta\eta_{j+1} + b_j^*Q_{j+1} = \left(c_j^* + d_j^*E_j\right)\Delta\eta_j^n + d_j^*F_j + G_j^* \quad (29)$$

From Equation 28, the following is acquired:

$$\Delta\eta_j = \frac{a_j}{c_j + d_jE_j}\Delta\eta_{j+1} + \frac{b_j}{c_j + d_jE_j}\Delta Q_{j+1} - \frac{d_jF_j + G_j}{c_j + d_jE_j} \quad (30)$$

And from Equation 30, the following is abstracted:

$$\Delta\eta_j = \frac{a_j^*}{c_j^* + d_j^*E_j}\Delta\eta_{j+1} + \frac{b_j^*}{c_j^* + d_j^*E_j}\Delta Q_{j+1} - \frac{d_j^*F_j + G_j^*}{c_j^* + d_j^*E_j} \quad (31)$$

When Equation 28 is subtracted from Equation 29, then:

$$\left\{a_j(c_j^* + d_j^*E_j) - a_j^*(c_j + d_jE_j)\right\}\Delta\eta_{j+1} + \left\{b_j(c_j^* + d_j^*E_j) - b_j^*(c_j + d_jE_j)\right\}\Delta Q_{j+1} = (d_jF_j + G_j)(c_j^* + d_j^*E_j) - (d_j^*F_j + G_j^*)(c_j + d_jE_j) \quad (32)$$

It is important to note that Equation 32 is identical with ΔQ_{j+1} = $E_{j+1}\Delta\eta_{j+1} + F_{j+1}$, then:

$$\Delta Q_{j+1} = -\frac{\left\{a_j(c_j^* + d_j^* E_j) - a_j^*(c_j + d_j E_j)\right\}\Delta\eta j+1}{\left\{b_j(c_j^* + d_j^* E_j) - b_j^*(c_j + d_j E_j)\right\}} + \frac{(d_j F_j + G_j)(c_j^* + d_j^* E_j) - (d_j^* F_j + G_j^*)(c_j + d_j E_j)}{\left\{b_j(c_j^* + d_j^* E_j) - b_j^*(c_j + d_j E_j)\right\}} \quad (33)$$

Therefore:

$$E_{j+1} = -\frac{\left\{a_j(c_j^* + d_j^* E_j) - a_j^*(c_j + d_j E_j)\right\}}{\left\{b_j(c_j^* + d_j^* E_j) - b_j^*(c_j + d_j E_j)\right\}} \quad (34)$$

$$F_{j+1} = \frac{(d_j F_j + G_j)(c_j^* + d_j^* E_j) - (d_j^* F_j + G_j^*)(c_j + d_j E_j)}{\left\{b_j(c_j^* + d_j^* E_j) - b_j^*(c_j + d_j E_j)\right\}} \quad (35)$$

The values of E_{j+1} and F_{j+1} depend on that of E_j and F_j, and this numerical solution requires two boundary conditions which include upstream and downstream. Therefore, there are three possible conditions, namely tidal $\eta(t)$, hydrograph $Q(t)$, and rating curve $Q(\eta)$ which are explained in the following boundary conditions.

- If $\eta(t)$ is given as a boundary condition, then:

$$\Delta Q_1 = E_1\Delta\eta_1 + F_1 \quad (36)$$

$$\Delta\eta_1 = \frac{\Delta Q_1}{E_1} - \frac{F_1}{E_1} \quad (37)$$

Letting $\Delta\eta_1$ be independent from $\frac{\Delta Q_1}{E_1}$, the value of $\frac{\Delta Q_1}{E_1} \approx 0$, and therefore, E_1 = -a is taken, where $a \approx 10^4$ - 10^6 and F_1 = -$a\Delta\eta_1$ = -a $(\eta_{j+1}^{n+1} - \eta_1^n)$.

- If $Q(\eta)$ is given as a boundary condition, then:

$$\Delta Q_1 = E_1\Delta\eta_1 + F_1, E_1 = 0, F_1 = (\Delta Q_1) = (Q_1^{n+1} - Q_1^n) \quad (38)$$

- If $Q(\eta)$ is given as a boundary, then:

$$\Delta Q_1 = E_1\Delta\eta_1 + F_1 \quad (39)$$

Applying the Taylor series, where $Q(t+\Delta t) = Q(t) + \Delta Q$ or $Q(t+\Delta t) = Q(\eta) + \frac{\partial Q(\eta)}{\partial\eta}\Delta\eta$, the following is gotten:

$$Q(t) + \Delta Q = Q(\eta) + \frac{\partial Q(\eta)}{\partial\eta}\Delta\eta \quad (40)$$

$$\Delta Q_1 = -Q_1^n + Q_1^n + \frac{\partial Q_1^n}{\partial\eta_1}\Delta\eta_1 \quad (41)$$

E_1 = $\frac{\partial Q_1^n}{\partial\eta_1}$, F_1 = 0

The three methods above are used to determine the value of E_1 and F_1. Meanwhile, the following conditions must be satisfied to determine $\Delta\eta$ and ΔQ:

- If $\eta(t)$ is given as a boundary condition, then:

$$\Delta\eta_j = \eta_j^{n+1} - \eta_j^n \quad (42)$$

- If $Q(t)$ is given as a boundary condition, then:

$$\Delta\eta_j = \frac{(\Delta Q_j - F_j)}{E_j} \quad (43)$$

The double sweep method for the Preissmann scheme is expressed as follow:

$$a_j\eta_{j+1} + b_j\Delta Q_{j+1} = c_j\Delta\eta_j + d_j\Delta Q_j + G_j \quad (44)$$

$$a_j^*\Delta\eta_{j+1} + b_j^*\Delta Q_{j+1} = c_j^*\Delta\eta_j + d_j^*\Delta Q_j + G_j^* \quad (45)$$

The two equations above are elimated by ΔQ_j such that

$$\Delta Q_j = \frac{(a_j\Delta\eta_{j+1} + b_j\Delta Q_{j+1} - c_j\Delta\eta_j - G_j}{d_j} \quad (46)$$

$$\Delta Q_j = \frac{a_j^*\Delta\eta_{j+1} + b_j^*\Delta Q_{j+1} - c_j^*\Delta\eta_j - G_j^*}{d_j^*} \quad (47)$$

Equation 46 is substracted by Equation 47, then:

$$\left(a_j d_j^* - a_j^* d_j\right)\Delta\eta_{j+1} + \left(b_j d_j^* - b_j^* d_j\right)\Delta Q_{j+1} - \left(c_j d_j^* - c_j^* d_j\right)\Delta\eta_j - \left(G_j d_j^* - G_j^* d_j\right) = 0 \quad (48)$$

$$\Delta\eta_j = \frac{(a_j d_j^* - a_j^* d_j)}{(c_j d_j^* - c_j^* d_j)}\Delta\eta_{j+1} + \frac{(b_j d_j^* - b_j^* d_j)}{(c_j d_j^* - c_j^* d_j)} \Delta Q_{j+1} - \frac{(G_j d_j^* - G_j^* d_j)}{(c_j d_j^* - c_j^* d_j)} = 0 \tag{49}$$

Equation 49 is changed to:

$$\Delta\eta_j = V_j\Delta\eta_{j+1} + W_j\Delta Q_{j+1} + X_j \tag{50}$$

The proposed correlation is written as:

$$\Delta Q_j = E_j\Delta\eta_j + F_j \tag{51}$$

$$a_j\eta_{j+1} + b_j\Delta Q_{j+1} = c_j\left(V_j\Delta\eta_{j+1} + W_j\Delta Q_{j+1} + X_j\right) + d_j\left(E_j\Delta\eta_j + F_j\right) + G_j \tag{52}$$

$$a_j\eta_{j+1} + b_j\Delta Q_{j+1} = c_jV_j\Delta\eta_{j+1} + c_jW_j\Delta Q_j + c_jX_j + d_jE_j \left(V_j\Delta\eta_{j+1} + W_j\Delta Q_{j+1} + X_j\right) + d_jF_j + G_j \tag{53}$$

$$(a_j - c_jV_j - d_jE_jV_j)\Delta\eta_{j+1} + (b_j - c_jW_j - d_jE_jW_j) \Delta Q_{j+1} = c_jX_j + d_jE_jX_j + d_jF_j + G_j \tag{54}$$

Equation 54 is changed to the form of $\Delta Q_{j+1} = E_{j+1}\Delta\eta_{j+1} + F_{j+1}$, where:

$$\Delta Q_{j+1} = \frac{-(a_j - c_jV_j - d_jE_jV_j)}{b_j - c_jW_j - d_jE_jW_j} = \frac{-a_j + c_jV_j + d_jE_jV_j}{b_j - c_jW_j - d_jE_jW_j} = \frac{V_j(c_j + d_jE_j) - a_j}{b_j - W_j(c_j + d_jE_j)} \tag{55}$$

$$\Delta Q_{j+1} = \frac{c_jX_j + d_jE_jX_j + d_jF_j + G_j}{b_j - c_jW_j - d_jE_jW_j} = \frac{X_j(c_j + d_jE_j) + d_jF_j + G_j}{b_j - W_j(c_j + d_jE_j)} \tag{56}$$

3 RESULT

3.1 Case 1: Rectangular Channel with Tidal Force

The channel is rectangular with 5,000 m and 1,000 m length and width, respectively. A tidal force with an amplitude of 2.5 m is applied at the channel upstream with a period of 12 hours, while the downstream is closed. The initial depth is 10 m for cold start condition without any slope, and the analytical solutions for the depth and velocity are written as:

$$\eta = \frac{a}{\cos\left(\frac{2\pi L}{\sqrt{gh}}\right)} \sin\left(\frac{2\pi L}{\sqrt{\text{gh}}}\left[\frac{x}{L} - 1\right]\right) \sin\left(2\pi t\right) \tag{57}$$

$$u = \frac{-a\sqrt{gh}}{h\cos\left(\frac{2\pi L}{\sqrt{gh}}\right)} \sin\left(\frac{2\pi L}{\sqrt{gh}}\left[\frac{x}{L} - 1\right]\right) \cos\left(2\pi t\right) \tag{58}$$

where a, L, 2π, t, η, and u represent amplitude, length of the channel, tidal frequency, time, wave height, and wave velocity, respectively.

The domain is discretized into 200 segments in the x-direction and was simulated for 24 hours. Figure 3 shows the analytical result versus the numerical model at x = 2,500 m. The average error rates from the analytical result for water depth and velocity, are 1.81% and 1.175%, respectively which indicated that the numerical model is quite accurate.

3.2 Case 2: Roll wave in a Rectangular Channel

A rectangular channel having a length of 24.4 m with a slope and width of 0.1201 m and 0.1175 m respectively, was used to produce periodic permanent roll waves. Its normal depth is 0.0053 m and the amplitude of the perturbations imposed at the inlet of the channel is 0.5%. According to Cao et al. (2015), steady water discharge of 8.02 x 10-4 m3/s is given at the inlet and the water depth is set as:

$$h_{in} = h_n + h_{am} sin(2\pi t/T) \tag{59}$$

where h_n is the normal depth, the perturbation

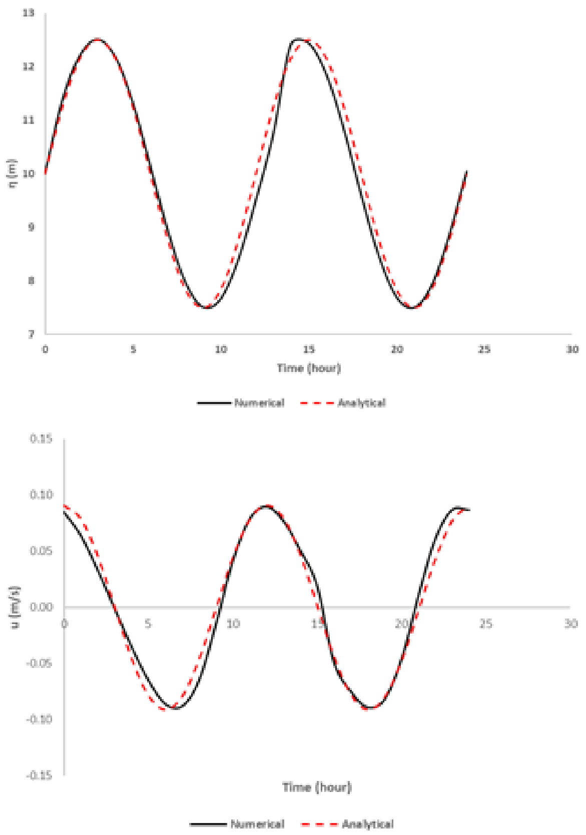

Figure 3 Case 1: Comparison of Numerical and Analytical Results for Water Depth and Velocity

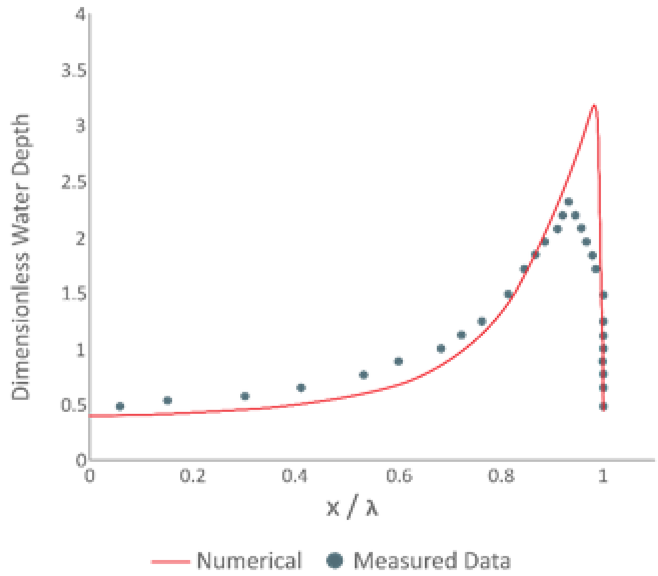

Figure 4 Case 2: Comparison of the Computed Water Depth and Measured Data from Brock (1967)

amplitude h_am =0.5% of h_n, and T refers to the perturbation period imposed at the inlet of the channel. The computational value is set in such a way that the forward wave does not reach the downstream boundary within the time of computation as conducted by (Cao et al., 2015). A dimensionless water depth is defined as h^*=h/h_n and the spatial step is set to be 0.001 m with a Courant number of 2. Figure 4 shows that the numerical model exhibits a stable performance, and the deviations are still considerable from the measured data originally performed by (Brock, 1967).

3.3 Case 3: Solitary Wave in a Channel

There has been no change in the shape and velocity of the wave traveling on the flat channel because friction and viscosity are not considered. Therefore, this case aims to simulate a solitary wave on a flat and frictionless channel. According to Kang and Jing (2017) and Stelling and Zijlema (2003) the water elevation and velocities are analytically expressed as:

$$\eta = asech^2\left(\sqrt{\frac{3a}{4d^3}}(x-ct)\right) \tag{60}$$

$$u = c\frac{\eta - d}{h} \tag{61}$$

where a is the amplitude, d is the water depth, and c = $\sqrt{g\left(d+a\right)}$. Equation 60 and Equation 61 are applied as an initial condition with a = 2 m and d = 10 m for Case 3a and a = 4 m and d = 10 m for Case 3b. The length of the channel is set to be 600 m, while the width is 5 m. The domain is discretized into 1,200 segments in the x-direction and the total simulation time is set to 30 s. These results of the simulation for both cases are seen in Figure 5 and Figure 6, respectively.

From both simulations, it was discovered that the decrease in water level occurs constantly, and in case 3a with α = 2 m as shown in Figure 5, the maximum drop occurs by 45%, while in Case 3b with α = 4 m represented in Figure 6, the maximum drop occurs by 75%. These results indicated that when the amplitude increases, the water level decreases, specifically in the second wave, and also showed that there is a significant difference between the analytical results and the numerical model due to the dispersion effect that is not considered in the SWE.

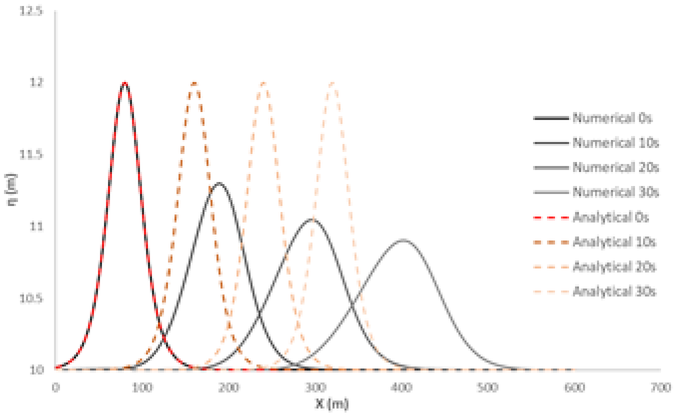

Figure 5 Case 3a: Comparison of Numerical and Analytical

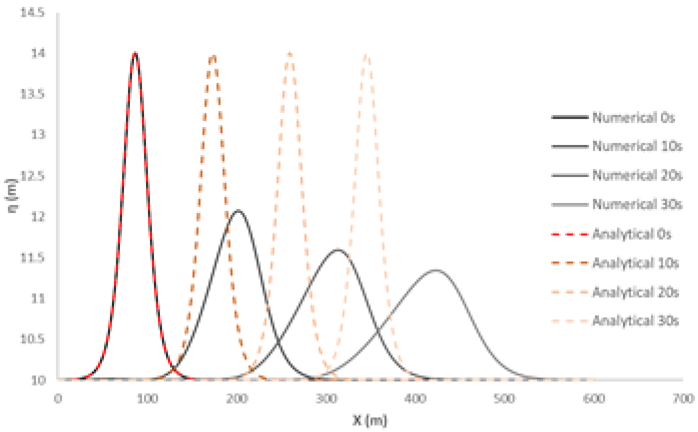

Figure 6 Case 3b: Comparison of Numerical and Analytical Results for Water Level

4 DISCUSSION

The simulation of three different types of wave propagation has demonstrated the capabilities of the Preissmann scheme. The first case is tidal wave propagation which shows the Preissmann scheme is quite accurate for longwave simulation. This was observed in the accurate prediction of both maximum water elevation and velocity, where the dispersion effect is insignificant, and the vertical velocity is uniform, thereby having the hydrostatic pressure distribution.

The second case is the rolling wave simulation which indicates the results of the Preissmann scheme are still consistent with the observed data for periodically-permanent wave propagation, although the wave crest is slightly overestimated. According to Cao et al. (2015), the dispersion's absence is independent of SWE numerical model's failure to capture wave crests because when this effect was added to the non-uniform vertical velocity distribution in the SWE, no significant change was observed in peak's position. This leads to the conclusion that dispersion is not a viable approach to improving the modeling accuracy of the permanent roll waves. However, when the turbulent term was included, the numerical accuracy increased significantly.

The third case, related to the solitary wave simulation shows that the model has significant discrepancies from the analytical solution, as expected. The dispersion effect for this benchmark case is considered large, and therefore the vertical-length scale becomes significant with respect to that of horizontal-length, to an extent that the non-hydrostatic effect has to be considered. In these present findings, neglecting the dispersion term causes the Peissmann scheme to underestimate the wave crest along with time. Meanwhile, the central difference scheme used in (Kang and Jing, 2017), found that the peak wave is overestimated and the wave occurrence position deviates.

In the research conducted by Ginting and Ginting (2020), the dispersion and non-dispersion shallow water models were compared to simulate the third case and a similar result with this current work was observed where the non-dispersion model underestimated the peak wave, indicating that it plays an important role. Based on the aforementioned phenomena, future study needs to investigate the accuracy of the Preissmann scheme with the turbulence and dispersion terms. This is achieved by adding such terms into the momentum equations of the SWE as follows:

$$\frac{\partial Q}{\partial t}+\frac{\partial}{\partial x}\left(\frac{Q^2}{A}\right)+gA\frac{\partial \eta}{\partial x}-gAS_0+gA\frac{Q|Q|}{K} = \frac{\partial(\eta T_R)}{\partial x}-\frac{\partial D}{\partial x} \quad (62)$$

where T_R is the depth-averaged Reynold stress and D is the dispersion momentum transport.

5 CONCLUSIONS

The three different types of propagation that have been modeled in this framework of the 1D SWE using Preissmann's implicit scheme include tidal, roll, and solitary waves. In the tidal wave simulation with a small dispersion effect, it was found that the Preissmann scheme accurately predicts both the water elevation and velocity. Also, in the second scope of the modeling where the dispersion plays a considerable role, the scheme was accurate in capturing the wave crest. When considering the turbulent-dominated case, the Preissmann scheme overestimated the wave peak but the occurrence positions were generally well-predicted. Moreover, in the solitary wave simulation, it was observed that the wave peaks and their occurrence positions were underestimated by the Preissmann scheme. This further explained that as the wave amplitude increases, the effect of the dispersion is more felt, thereby causing the numerical model to be less accurate. In the future, it would be interesting to investigate the simulation of the SWE model with the Preissmann scheme including the dispersion and the turbulence terms.

DISCLAIMER

The authors declared no conflict of interest nor personal relationships which can affect the work reported in this research.

AVAILABILITY OF DATA AND MATERIALS

All data are available from the author.

ACKNOWLEDGMENTS

The authors are grateful specifically to the Research Institution and Community Service (Lembaga Penelitian dan Pengabdian Kepada Masyarakat), Parahyangan Catholic University for releasing grants with the contract number: III/LPPM/2021-08/155-P.

REFERENCES

An, H., Lee, S., Noh, S. J., Kim, Y. and Noh, J. (2018), 'Hybrid numerical scheme of preissmann slot model for transient mixed flows', *Water* **10**(7), 899.

Arcos, M. E. M. and LeVeque, R. J. (2015), 'Validating velocities in the geoclaw tsunami model using observations near hawaii from the 2011 tohoku tsunami', *Pure and Applied Geophysics* **172**(3), 849–867.

Audusse, E., Steinstraesser, J. G. C., Emerald, L., Heinrich, P., Paris, A. and Parisot, M. (2019), Comparison of models for the simulation of landslide generated tsunamis, *in* 'ESAIM: Proceedings'.

Brock, R. R. (1967), 'Development of roll waves in open channels'.

Brunner, G. and USACE (2016), 'Hec-ras river analysis system hydraulic reference manual. version 5.0', *Hydrol. Eng. Cent.(HEC), US Army Corps Engineering* .

Cao, Z., Hu, P., Hu, K., Pender, G. and Liu, Q. (2015), 'Modelling roll waves with shallow water equations and turbulent closure', *Journal of Hydraulic Research* **53**(2), 161–177.

Chollet, J.-P. and Cunge, J. A. (1980), 'Simulation of unsteady flow in alluvial streams', *Applied Mathematical Modelling* **4**(4), 234–244.

Clemmens, A., Holly Jr, F. and Schuurmans, W. (1993), 'Description and evaluation of program: Duflow', *Journal of irrigation and drainage engineering* **119**(4), 724–734.

Ginting, B. M. and Ginting, H. (2020), 'Extension of artificial viscosity technique for solving 2d non-hydrostatic shallow water equations', *European Journal of Mechanics-B/Fluids* **80**, 92–111.

Ginting, B. M. and Mundani, R.-P. (2019), 'Comparison of shallow water solvers: applications for dam-break and tsunami cases with reordering strategy for efficient vectorization on modern hardware', *Water* **11**(4), 639.

Kang, L. and Jing, Z. (2017), 'Depth-averaged non-hydrostatic hydrodynamic model using a new multithreading parallel computing method', *Water* **9**(3), 184.

Meister, O., Rahnema, K. and Bader, M. (2016), 'Parallel memory-efficient adaptive mesh refinement on structured triangular meshes with billions of grid cells', *ACM Transactions on Mathematical Software (TOMS)* **43**(3), 1–27.

Pratomo, Y., Pranowo, W. S. and Setiadi, H. (2016), 'Identifikasi penjalaran gelombang panjang samudera hindia ke selat lombok berdasarkan komponen harmonik arus', *Omni-Akuatika* **12**(1).

Sart, C., Baume, J.-P., Malaterre, P.-O. and Guinot, V. (2010), 'Adaptation of preissmann's scheme for transcritical open channel flows', *Journal of Hydraulic Research* **48**(4), 428–440.

Sorensen, R. M. (2006), 'Basic coastal engineering', *New York, USA, Springer* .

Stelling, G. and Zijlema, M. (2003), 'An accurate and efficient finite-difference algorithm for non-hydrostatic free-surface flow with application to wave propagation', *International journal for numerical methods in fluids* **43**(1), 1–23.

[This page is intentionally left blank]